Research Article

Omar H. Hassoon*, Mayyadah S. Abed, Jawad K. Oleiwi, and M. Tarfaoui

# Experimental and numerical investigation of drop weight impact of aramid and UHMWPE reinforced epoxy

https://doi.org/10.1515/jmbm-2022-0008
Received Nov 22, 2021; accepted Mar 10, 2022

**Abstract:** Due to their characteristics such as weight/strength ratio and absorbed energy, the widespread use of composite materials in the last decades engorged the companies to exploit these materials invariant applications like the aerospace, automobile, and marine hull. However, there are some obstructs to the use of these materials that may constrain that. This came from the fact, that composite materials suffer from different damages modes that occur during loading and can be lead to catastrophic failure in their structure, such as intralaminar and interlaminar damage. Consequently, this motivated the researchers to study its behavior considering different damage modes and at different loading states. This work performed a finite element simulation using the Abaqus program of low-velocity drop impact for epoxy reinforced with Kevlar 49 and Ultra High Molecular Weight Polyethylene (UHMWPE) with different thicknesses and number of layers. A user-defined material VUMAT subroutine-based progressive damage model, and the Hashin failure criteria implemented in Abaqus Explicit finite element code had been utilized in this work. In Addition, the interlaminar damage models depend on the cohesive zone model (CZM). The numerical simulation results were compared with the experiments data to confirm the reliability of the numerical model.

**Keywords:** Low-velocity impact, laminated composites, damage modes, drop weight impact, Finite elements method

***Corresponding Author: Omar H. Hassoon:** Department of Production Engineering and Metallurgy, University of Technology, Baghdad, Iraq; Email: omar.h.hassoon@uotechnology.edu.iq
ORCID: 0000-0002-4695-1894
**Mayyadah S. Abed, Jawad K. Oleiwi:** Department of Materials Engineering, University of Technology, Baghdad, Iraq
**M. Tarfaoui:** ENSTA Bretagne, IRDL, UMR CNRS 6027, F-29200 Brest, France; Green Energy Park-IRESEN/UM6P, km2 R206 Benguerir, Morocco

## 1 Introduction

The composite materials have been used in many applications in recent decades due to their exclusive properties such as the safety and defense industries as body armor, helmets, and shielding vehicles. For example, human bodies may be shot or struck by explosion debris; a car may crash, aircraft engine turbines hit by birds, or tires hit during takeoff or landing. Dropped tools may also cause impact damage during fabrication or maintenance. Laminated composites are more likely to affect damage when compared with the bulk of some metals [1–5].

Impact damage is not usually a hazard in metallic structures since significant quantities of energy can be absorbed due to the ductility of this material. So, at yield stress, the metal may flow at a steady yield before hardening for huge strains (up to 20 percent). Composites, by contrast, can fail in different modes and cause barely detectable impact damage (BVID), which also significantly decreases the component's integrity. In general, most composites behave as a brittle material, and therefore elastic deformation is the only mechanism of damage to absorb energy, not through plastic deformation. At the same time, the term damage resistance refers to the magnitude of damage from the impact that is caused [6].

Composites are widely used in the safety and defense industries as body armor, helmets, and shielding vehicles [7, 8] due to their desirable damage resistance, laminar strengths, low cost and multifunctional design capability [9, 10] high strength-to-weight ratio, good fatigue resistance, damping characteristics, high corrosion resistance. These composites commonly withstand impact loads from low to even hyper-velocity through their service life [11]. For this reason, composite materials need a detailed study when applying dynamic loading on composite materials to achieve greater protection [7].

Impact behavior is sensitive to the structure of the composite, the fiber volume fraction, the dimension of the whole composite, and laminate number. So the high-performance fiber practically influences the compression

and impact properties [9]. The most popular laminated composites used in armor design are fabricated from high-strength, high-modulus polymeric fibers as a woven fabric like aramid and UHMWPE in the resin matrix. Kevlar is the most influential fiber that helps in different defense equipment like tanks, helicopters, and body armor as a protective shield. In this application, its essential duty is to prevent the object's perforation or surface fragments [12].

Kevlar is one of the most commonly used artificial woven fabrics in the armors. The polymerization process makes it. Aramid is an excellent substance for armor because it has high tensile strength, high strength/weight ratio, is stronger and tougher than steel alloy, and is capable of absorbing energy compared to other materials [13]. In the last two decades, composites reinforced with ultra-high molecular weight polyethylene fiber have gained significant importance for armor and structural applications due to their high-absorbed energy due to dynamic load, and excellent specific strength [14].

Schoeppner and Abrate (2000) determined the laminated composite delamination threshold loads through low-velocity impact from the load-displacement or load–time plot. So the sudden drop in load causes reducing in stiffness of the specimen due to laminate level damage. About 500 Low-Speed, Load-Time Impact Database is utilized to determine the load threshold for delamination. The database includes impact test data of laminate fabricated from graphite/PEEK, graphite/epoxy, and graphite/BMI material. Finally, C-scan damage measurements were also executed to compare observations of delamination threshold load of the affected specimens [15].

Yang *et al.* (2015) studied experimentally and numerically a low-velocity impact of interply hybrid composites based on glass and carbon woven fabrics that reinforced polymerized polybutylene terephthalate. The finite element method and experiment were executed to determine the hybridization influence on the composites at impact speeds of 3.5 and 7 m/s, respectively. Specimens were prepared using the vacuum-assisted prepregs method. Experimental research determined all the parameters of the material used in the simulation. In ABAQUS/Explicit, 3D finite element models were improved to determine the damage behavior. Experimental findings indicate that hybrid composites at a 37/63 mass ratio consume more energy in the impact test relative to single-phase composites, and the perforation thresholds dramatically improve. The findings of the test are well in line with the experimental tests. The damage mode of low-velocity-impact interplay hybrid composites is further addressed [16].

Meshi *et al.* (2016) investigated the delamination behavior of the UHMWPE reinforced soft polymer matrix. Two experimental setups for UHMWPE composites are being suggested and investigated, the modified Double Cantilever Beam test and a new interlaminar shear (ILS) test. The latter was suggested to describe delamination failure in Mode-II, which is due to a weak matrix-fiber interphase bond. The Digital Image Correlation approach is used to derive and analyze the uniformity of the maximum field shear strain in Mode-II. In mode-I crack, length has also been quantified using optical means [17].

Fadhil *et al.* (2016) used different weight percentages of multi-walled carbon nanotubes for epoxy reinforcement. Drop-weight impact and tensile measures were utilized to determine the mechanical properties of the composites. The results showed that 0.2% of CNTs enhanced tensile characteristics, while 0.6% of CNTs developed impact properties [18]. Ahmed (2016) used various impactor designs to carry out tower impactors (cone, bullet, and hemispheric). This study evaluates the impact characteristics using unidirectional carbon, unidirectional glass, woven glass, and hybrid (carbon + glass) reinforced epoxy composites. The experimental results revealed that impactor design change does not affect the impact characteristics of woven fiber-reinforced composite, while it had a significant influence on unidirectional fiber-reinforced composites [19].

Sy (2017) tested low-velocity impact loading of flax reinforced epoxy composite laminates using passive Infra-Red thermography to monitor the damage evolution through impact tests. It evaluated two configurations: unidirectional and cross-ply. The unidirectional laminate showed a weak, brittle response to the effect. In comparison, the cross-ply laminate significantly affected impact; energy penetration reached three times higher than the unidirectional and tougher 2.5 times higher. Additional tests were carried out to assess the effect of Kevlar49 hybridizations. Test results showed substantial improvement in unidirectional flax/epoxy laminate impact efficiency. Hybridization increased three times its threshold of energy penetration. It decreased the cross-ply flax/epoxy laminate penetration threshold by 10 percent; however, it doubled the toughness. The Kevlar-Flax/epoxy laminates' impact toughness was slightly higher than aluminum and CFRP's, making them sustainable alternatives for impact applications [20].

Nachtane *et al.* (2018) investigated numerically the durability of a ducted tidal turbine made from composite materials (Carbon-epoxy/Glass-polyester) under impact loading and their damage behavior. The numerical model included the composite materials damage initiation criteria and progressive using user-subroutine (VUMAT). In addition, the numerical model takes into consideration hydrostatic and hydrodynamic loads [21].

Hu *et al.* (2019) tried to study the effect of the toughening mechanism by Kevlar short fiber reinforced carbon fiber composite laminates through a low-velocity impact test using a drop-weight impact system. After a low-velocity impact check, industrial computed tomography and Ultrasonic C-scan exposed the internal damage, complete damage, and distribution damage. Mechanical behaviors of carbon-reinforced plastics were analyzed in-depth depending on the energy absorption and the complex effect responses. Besides, carbon fiber reinforced polymers with and without chopped Kevlar fiber were examined for residual compression strength and failure pressure. They showed no obvious advantages of toughened laminates at lower energy impact, but the strengths of compression-after-impact and the stress values of failure enhanced during a varied range of energy with chopped Kevlar fiber. To clarify the experimental results and related mechanisms, 3D distribution of internal damage and SEM were used along with fracture toughness analysis [22].

Nachtane *et al.* (2020) studied numerically the influence of environmental exposure of composite (GFRP) tidal turbine and under impact loading. The three-dimensional finite element model has been used and performed using Explicit/Abaqus software. Different loading (hydrostatic and hydrodynamic) was applied in the model. Also, the damage behavior of the tidal composite material was integrated into the numerical model using a user subroutine (VUMAT) for both damage initiation and progressive [23].

Gürgen (2020) fabricated UHMWPE samples in a compression molding and then varied its parameters such as temperature and pressure during the fabrication to study the impact performance influence of molding parameters. However, the UHMWPE matrix contained silicon carbide fillers to improve the impact resistance of the samples. The results showed that the molding temperature above the melting point of the polymer exhibited anti-impact behavior. Also, carbide fillers enhanced the frictional interaction between the composites and impactors, enhancing the impact resistance [24]. Abed *et al.* (2020) made a comparison between composites made off 12 and 20 layers of aramid fabrics and UHMWPE woven fabrics reinforced epoxy through Izod impact and drop-weight impact. The composite based on Kevlar revealed composite damage by fiber and matrix breakages during the Izod test. Whereas delamination was noticed in UHMWPE reinforced epoxy (PE). For Kevlar-reinforced epoxy, the average impact strength rises with the number of laminates [25].

Recently, Maziz *et al.* (2021) presented numerical and analytical models for modeling the mechanical behavior of the pressurized tubular structures. A good approximation was observed using these models when comparing the experimental data with the numerical and analytical results. The ability of this model to simulate the mechanical properties of the tubular composites subjected to internal pressure was demonstrated [26].

The main objective of this study is to model an appropriate finite element simulation using the Abaqus program and integrate some failure modes that occur in composite materials during low-velocity drop experiments. This study was conducted for epoxy reinforced with aramid and Ultra High Molecular Weight Polyethylene (UHMWPE) at different thicknesses and number of layers to evaluate the numerical model's reliability.

# 2 Experimental setup

## 2.1 Specimen fabrication

The laminate investigated in this work was fabricated by two different woven fabrics, Kevlar 49 and UHMWPE woven fabric; the fiber properties are summarized in Table 1. The matrix epoxy was applied from Sika AG. The epoxy resin consists of low viscosity and solvent-free epoxy resin components, which have mechanical properties compressive strength ~95 N/mm$^2$, Shore D hardness 83, and flexural strength ~30 N/mm$^2$. The composite laminate was fabricated by hand layup process with two different thicknesses (12 and 20) for each type of Kevlar-epoxy and UHMWPE-epoxy composites [23]. The specimens tested are described in Table 2.

**Table 1:** Woven fabric Properties (UHMWPE and Kevlar 49) [23]

| Property | UHMWPE fiber | Kevlar 49 |
|---|---|---|
| Density (g/cm$^3$) | 0.97–0.98 | 1.45 |
| Tensile strength (cN/tex) | 285.6–408 | 200 |
| Tensile modulus (cN/tex) | 9282–14280 | 8300 |
| Elongation at break (%) | 3.5–3.7 | 2.5 |
| Range of temperature (°C) | 80 | 204 |
| Temperature of decomposition (°C) | 145–160 | 400 |
| Strength retention at 300°C 100 h (%) | 68–70 | 60–65 |
| Moisture absorption (%) | 0.6 | 4.5 |
| Wear resistance | Good | General |
| Solvent resistance | Good | Good |
| Acid resistance | Good | Bad |
| Alkali resistance | Good | Good |
| UV resistance | Good | Bad |

**Table 2:** Specimens tested of composite material

| Number of specimens | Material type | N. of layers | Impact energy (J) | Type of weave fabric |
|---|---|---|---|---|
| 3 | UHMWPE-epoxy | 12 | 40 | Plain weave |
| 3 | UHMWPE-epoxy | 20 | 40 | Plain weave |
| 3 | Kevlar-epoxy | 12 | 40 | Plain weave |
| 3 | Kevlar-epoxy | 20 | 40 | Plain weave |


**Figure 1:** Drop weight impact machine

## 2.2 Low-velocity impact test

The low-velocity impact was carried out using a drop-weight impact machine (INSTRON 9350) [19], which is shown in Figure 1. Velocity and force sensors are computerized in the device to determine energy-time and force-time relationships automatically. The composite plate materials have a dimension of 150*100 mm and thickness (N*0.4 mm for Kevlar-epoxy) and (N*0.9 mm for UHMWPE-epoxy) where the N is the number of the layers. The impactor has a mass of 5.1 kg with a hemisphere tip at the end. The material of the impactor is made of steel (E = 210 Gpa, $\nu$ = 0.3). The reason behind using a hemispherical head is to more understand the damage behavior of composite materials, as this geometric can be occurred more damage compared to the flat-head, although the composite materials can suffer a higher maximum load when using

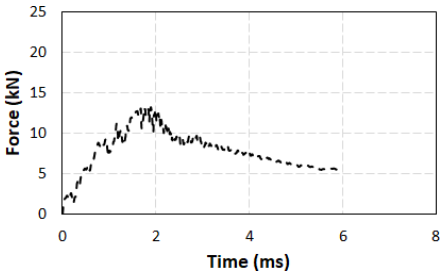


**(a)** 12-layers of Kevlar Reinforced Epoxy

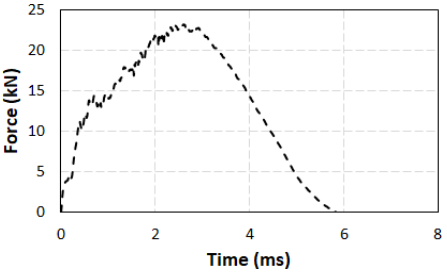


**(b)** 20-layers of Kevlar Reinforced Epoxy

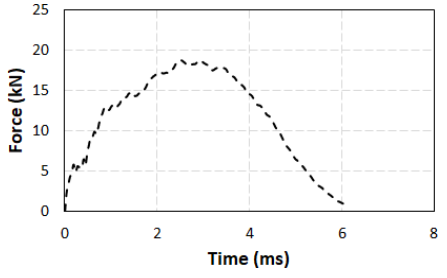


**(c)** 12-layers of UHMWPE Reinforced Epoxy

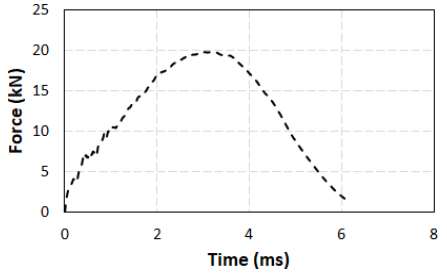


**(d)** 20-layers of UHMWPE Reinforced Epoxy

**Figure 2:** Force-Histories experimental results

a flat-head [27]. The plate is fully clamped at its external edges.

# 3 Experimental results

## 3.1 Force-time history

The obtained results are presented in Figure 2. The first results that can evaluate the drop test impact are the force-time histories; these can give an overview of the maximum strength of the composite plate against the impactor object. From these results, the composite plate with 12 layers of Kevlar Reinforced Epoxy has lower impact strength than UHMWPE Reinforced Epoxy.

# 4 Finite element numerical model

## 4.1 Model geometric and setup configuration

In this study, a numerical finite element model has been performed using Abaqus/Explicit to simulate a low-velocity impact for the Kevlar-epoxy and UHMWPE-epoxy. In the numerical model performed with the same conditions as that in the experimental work, the plate composite materials have a dimension of 150*100 mm and thickness (N*0.4 mm for Kevlar-epoxy) and (N*0.9 mm for UHMWPE-epoxy) where the N is the number of the layers. The impactor has a mass of 5.1 kg with a hemisphere tip at the end. The material of the impactor is made of steel (E = 210 Gpa, $\nu$ = 0.3). The plate is fully clamped at its external edges, as shown in Figure 3. For more accuracy of the stress and damage results, mesh convergence has performed, local refine meshing locate in the center of the plate as close to impact the region with mesh size (double seeds from min 1 mm to max 4 mm from the center to the outer edges) approximately. The total elements of the plate are 63480 linear hexahedral elements of type C3D8R and 60306 linear hexahedral elements, and the cohesive element is COH3D8 type. The Explicit general contact is defined between the impactor and the composite plate with hard contact (the clearance between adjacent surfaces is zero) and frictionless properties. The Dynamic Explicit step with automatic increment type was used.

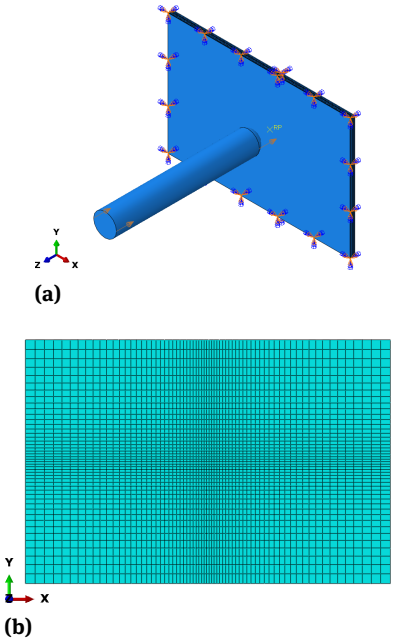


**Figure 3:** Finite element model (a) boundary condition (b) model meshing

## 4.2 Constitutive progressive degradation of intralaminar

The impact tests were simulated using finite element Explicit/Abaqus commercial code. The model adopted the progressive failure models to predict the initial damage and propagation in the composite materials depending on the continuum damage mechanics' concept (CDM). A user-defined subroutine (VUMAT) was integrated with Abaqus software to predict the damage in fiber and matrix. The material behavior consists of two distinct regions. The elastic region defines the material behavior as the materials return to the original shape as the load is removed. This region has an energy that depends on its material nature. The material behaves and intends to fail after this region, especially for many different composite materials without passing throughout the plastic region. The failure begins when it reaches damage onset. Consequently, the cracks become apparent with increasing loading, leading to degradation of material properties. The relation between effective stress ($\hat{\sigma}$) and nominal stress ($\sigma$) defines as:

$$\hat{\sigma} = d \cdot \sigma \tag{1}$$

Where $d$ is the damage operator

So the stress with damages presence is:

$$\sigma_{ij} = C_{ij}(d) \cdot \epsilon_{ij} \tag{2}$$

In which $C$ is the undamaged orthotropic stiffness matrix, which takes the following form:

$$C = \begin{bmatrix} C_{11} & C_{12} & C_{13} & 0 & 0 & 0 \\ C_{12} & C_{22} & C_{23} & 0 & 0 & 0 \\ C_{13} & C_{23} & C_{33} & 0 & 0 & 0 \\ 0 & 0 & 0 & C_{44} & 0 & 0 \\ 0 & 0 & 0 & 0 & C_{55} & 0 \\ 0 & 0 & 0 & 0 & 0 & C_{66} \end{bmatrix} \quad (3)$$

Then the damage stiffness matrix is as follows [28–30]:

$$dC_{11} = \left(1 - d_f\right) E_1 \left(1 - {\nu_{23}}^2\right) \Gamma, \quad (4)$$

$$dC_{33} = \left(1 - d_f\right)\left(1 - d_m\right) E_3 \left(1 - {\nu_{21}}^2\right) \Gamma,$$
$$dC_{23} = \left(1 - d_f\right)\left(1 - d_m\right) E_2 \left(\nu_{32} - \nu_{12}\nu_{31}\right) \Gamma,$$
$$dC_{44} = \left(1 - d_f\right)\left(1 - d_{mt}s_{mt}\right) E_1 \left(1 - d_{mc}s_{mc}\right) G_{12},$$
$$dC_{66} = \left(1 - d_f\right)\left(1 - d_{mt}s_{mt}\right) E_1 \left(1 - d_{mc}s_{mc}\right) G_{31},$$
$$dC_{22} = \left(1 - d_f\right)\left(1 - d_m\right) E_2 \left(1 - {\nu_{13}}^2\right) \Gamma,$$
$$dC_{12} = \left(1 - d_f\right)\left(1 - d_m\right) E_1 \left(\nu_{21} - \nu_{31}\nu_{23}\right) \Gamma,$$
$$dC_{31} = \left(1 - d_f\right)\left(1 - d_m\right) E_1 \left(\nu_{31} - \nu_{21}\nu_{32}\right) \Gamma,$$
$$dC_{55} = \left(1 - d_f\right)\left(1 - d_{mt}s_{mt}\right) E_1 \left(1 - d_{mc}s_{mc}\right) G_{23}$$

**Table 3:** Failure criteria

| Failure mode | Failure criteria |
|---|---|
| Fibre tensile failure ($\sigma_{11} \geq 0$) | $f_{ft} = \left(\frac{\sigma_{11}}{X_t}\right)^2 + \left(\frac{\sigma_{12}}{S_{12}}\right)^2 + \left(\frac{\sigma_{13}}{S_{13}}\right)^2 \geq 1$ |
| Fibre compression failure ($\sigma_{11} < 0$) | $f_{fc} = \left(\frac{\sigma_{11}}{X_c}\right)^2 \geq 1$ |
| Matrix tensile failure ($\sigma_{22} + \sigma_{33}) \geq 0$ | $f_{mt} = \frac{(\sigma_{22}+\sigma_{33})^2}{{Y_t}^2} + \frac{{\sigma_{23}}^2 - \sigma_{22}\sigma_{33}}{S_{23}^2} + \left(\frac{\sigma_{12}}{S_{12}}\right)^2 + \left(\frac{\sigma_{13}}{S_{13}}\right)^2 \geq 1$ |
| Matrix compression failure ($\sigma_{22} + \sigma_{33}) < 0$ | $f_{mc} = \frac{1}{Y_c}\left(\left(\frac{Y_c}{2S_{23}}\right)^2 - 1\right)(\sigma_{22} + \sigma_{33}) + \frac{(\sigma_{22}+\sigma_{33})^2}{4{S_{23}}^2} + \frac{{\sigma_{23}}^2 - \sigma_{22}\sigma_{33}}{S_{23}^2} + \left(\frac{\sigma_{12}}{S_{12}}\right)^2 + \left(\frac{\sigma_{13}}{S_{13}}\right)^2 \geq 1$ |

**Table 4:** Equivalent displacement and equivalent stress for each mode [32]

| Failure mode | $\delta_{i,eq}$ | $\sigma_{i,eq}$ |
|---|---|---|
| Fibre tensile damage mode | $L_c\sqrt{(\epsilon_{11})^2 + (\epsilon_{12})^2 + (\epsilon_{31})^2}$ | $\frac{L_c(\sigma_{11}\epsilon_{11} + \sigma_{12}\epsilon_{12} + \sigma_{31}\epsilon_{31})}{\delta_{1,eq}}$ |
| Fibre compressive damage mode | $L_c\sqrt{\left(-\epsilon_{11} - \frac{\langle\epsilon_{33}\rangle . E_{33}}{E_{11}}\right)^2}$ | $\frac{L_c(E_{11}(-\epsilon_{11} - \frac{\langle\epsilon_{33}\rangle . E_{33}}{E_{11}})}{\delta_{2,eq}}$ |
| Matrix tensile damage mode | $L_c\sqrt{(\epsilon_{22})^2 + (\epsilon_{12})^2 + (\epsilon_{23})^2}$ | $\frac{L_c(\sigma_{22}\epsilon_{22} + \sigma_{12}\epsilon_{12} + \sigma_{23}\epsilon_{23})}{\delta_{3,eq}}$ |
| Matrix compressive damage mode | $L_c\sqrt{\left(-\epsilon_{22} - \frac{\langle\epsilon_{33}\rangle . E_{33}}{E_{22}}\right)^2 + (\epsilon_{12})^2}$ | $\frac{L_c(E_{22}(-\epsilon_{22} - \frac{\langle\epsilon_{33}\rangle . E_{33}}{E_{22}} + \sigma_{12}\epsilon_{12})}{\delta_{2,eq}}$ |

Where $\delta_{i,eq}$, $\sigma_{i,eq}$ and $L_c$ are equivalent displacement, equivalent stress and characteristic length, respectively.

**Table 5:** Properties of woven Kevlar 49-Epoxy

| | Properties data | | | | | | | | |
|---|---|---|---|---|---|---|---|---|---|
| Elastic properties (Gpa) | $E_{11}$ | $E_{22}$ | $E_{33}$ | $\nu_{12}$ | $\nu_{23}$ | $\nu_{13}$ | $G_{12}$ | $G_{23}$ | $G_{31}$ |
| | 79.56 | 79.56 | 3.38 | 0.015 | 0.342 | 0.342 | 2 | 2 | 2 |
| Damage initiation (Mpa) | $X_t$ | $X_c$ | $Y_t$ | $Y_c$ | $Z_t$ | $Z_c$ | | | |
| | 2490 | 700 | 800 | 700 | 700 | 800 | | | |
| Damage evolution (N/mm) | $F_t$ | $F_c$ | $M_t$ | $M_c$ | | | | | |
| | 81.5 | 106.3 | 0.28 | 0.79 | | | | | |

where the damage parameters and $\Gamma$ are given by Eq. (5) [28, 29]

$$d_f = 1 - (1 - d_{ft})(1 - d_{fc})$$
$$d_m = 1 - (1 - d_{mt})(1 - d_{mc}) \quad (5)$$
$$\Gamma = \frac{1}{(1 - \nu_{12}{}^2 - \nu_{23}{}^2 - \nu_{13}{}^2 - 2\nu_{12}\nu_{23}\nu_{13})}$$

where $d_m$, $d_f$, and $d_s$ are the damage parameters for the matrix, fiber, and shear failure modes, respectively.

The initiation of damage is modeled based on failure onset, which depends on Hashin failure criteria. A user material VUMAT subroutine was programed in FORTRAN language and implemented by the finite element explicit Abaqus software to evaluate the intralaminar damage. Table 3 illustrates the damage criteria. As the initial failure criteria have been satisfied, and with more loading, the material's stiffness begins to regression. The damage evolution can be constituted based on the relationship between effective stress and displacement. This is illustrated in Table 4. The mechanical and intralaminar failure properties used in this numerical model are illustrated in Table 5.

## 4.3 Interlaminar damage model

The cohesive element is integrated into the simulation model to represent the interlaminar damage (delamination) between the plies in the composite materials. This type of damage is defined based on traction-separation constitutive law to represent the interface between the layers. The stress-based quadratic criterion describes damage onset. The debonding between plies satisfied the traction-separation law, as in Eq. (6) [31].

$$\left(\frac{t_n}{t_n^0}\right)^2 + \left(\frac{t_s}{t_s^0}\right)^2 + \left(\frac{t_t}{t_t^0}\right)^2 = 1 \quad (6)$$

The nominal traction stress and the $1^{st}$ and $2^{nd}$ shear stresses are represented as $t_n$, $t_s$, $t_t$, respectively. The delamination propagation depends on the dissipated energy through the separation of layers [33]. The total energy of

**Table 6:** Interlaminar properties of composite [34]

| *Interlaminar properties* | | | |
|---|---|---|---|
| Elastic properties E (MPa) | 2.8 | | |
| Mode I strength (MPa) | $\tau_1$ | $\tau_2$ | $\tau_3$ |
| | 43.8 | 26 | 26 |
| Fracture toughness (N/mm) | $G_{IC}$ | $G_{IIC}$ | $G_{IIIC}$ |
| | 0.643 | 0.905 | 0.905 |

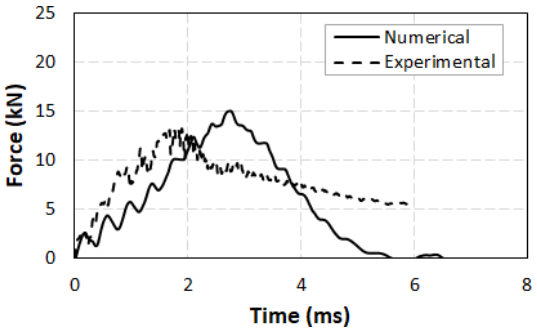


**(a)** 12-layers

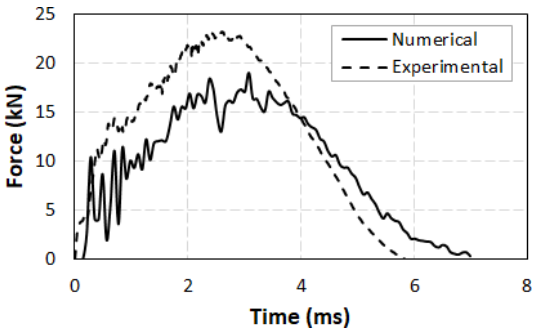


**(b)** 20-layers

**Figure 4:** Experimental and numerical force-time histories of Kevlar Reinforced Epoxy

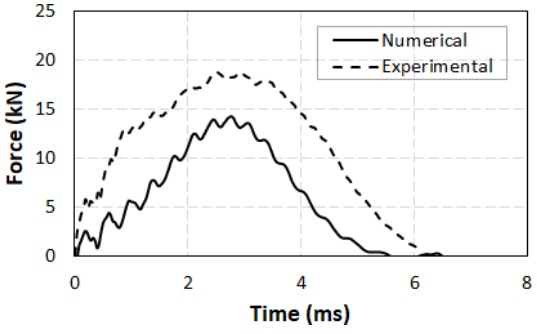


**(a)** 12-layers

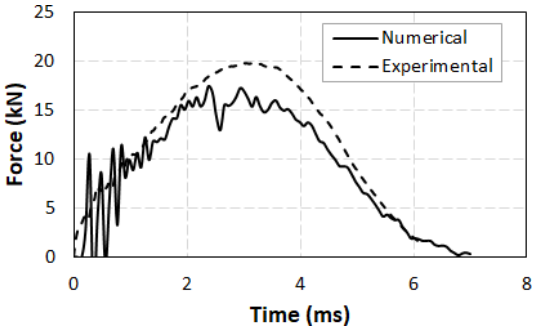


**(b)** 20-layers

**Figure 5:** Experimental and numerical force-time histories of UHMWPE Reinforced Epoxy

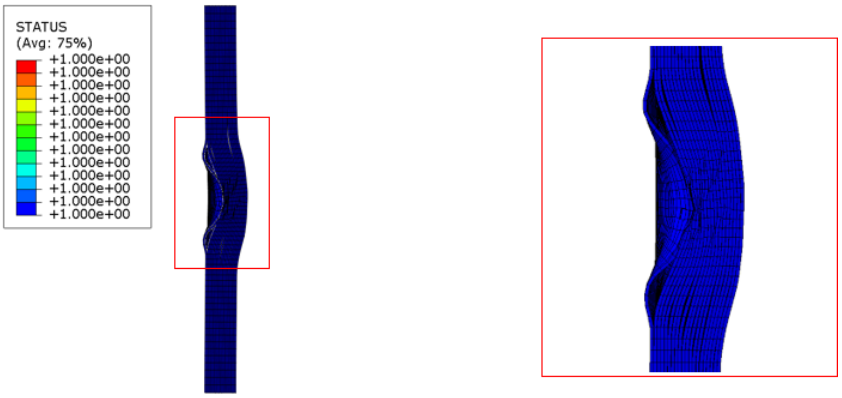


**Figure 6:** Interlaminar damage (delamination)

fracture is:

$$G_{Tc} = G_{Ic} + (G_{IIc} - G_{Ic}) \left( \frac{G_{II+}G_{III}}{G_T} \right)^{\eta} \tag{7}$$

where $G_T = G_I + G_{II} + G_{III}$
Where $G_{Tc}$: is the release rate of total critical energy
$G_{Ic}$: is the release rate of Mode I critical energy
$G_{IIc}$: is the release rate of Mode II critical energy
$G_T$: is the release rate of total energy, and
$\eta$: Material parameter

The damage variables utilized in simulations to feature the initiation and propagation of the cohesive interface as shown in Table 6.

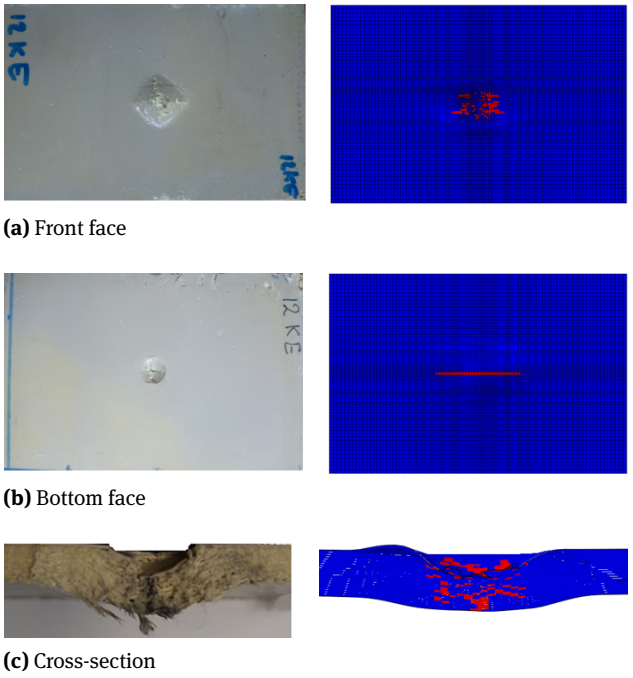

**(a)** Front face

**(b)** Bottom face

**(c)** Cross-section

**Figure 7:** Comparison between experimental numerical damage of Kevlar 12 plies reinforced epoxy

# 5 Results and discussion

## 5.1 Low-velocity impact test

The experimental and finite element simulation forces histories are compared in Figures 4 and 5 for the two studied material types and various thicknesses. Comparison of numerical results and experimental data is acceptable in predicting the force histories and the damage behavior. However, some differences in force magnitude can be attributed to the boundary conditions of the external edges that have been clamped perfectly in the numerical model, and perhaps some of the variables were ignored which occurred in an experimental study. The oscillation in the force-time histories attributes to the damage modes that happen in the composite materials. The delamination between the composite layers occurs firstly, making the composite plate more flexible; consequently, more vibration in the plate has been obvious.

## 5.2 Failure modes analysis

The failure modes during the low-velocity impact can be classified as their time that occurs through the degradation behavior of the composite materials. The failure mechanism begins when the crack appears in the composite plate and then propagates and develops between the layers. This led to another more significant damage mode known as the delamination, as shown in Figure 6. This type of damage makes the composite plate weaker due to the interface discontinuity of composite layers.

The comparison between experimental and numerical results of damage modes is obvious in Figure 7. Due to

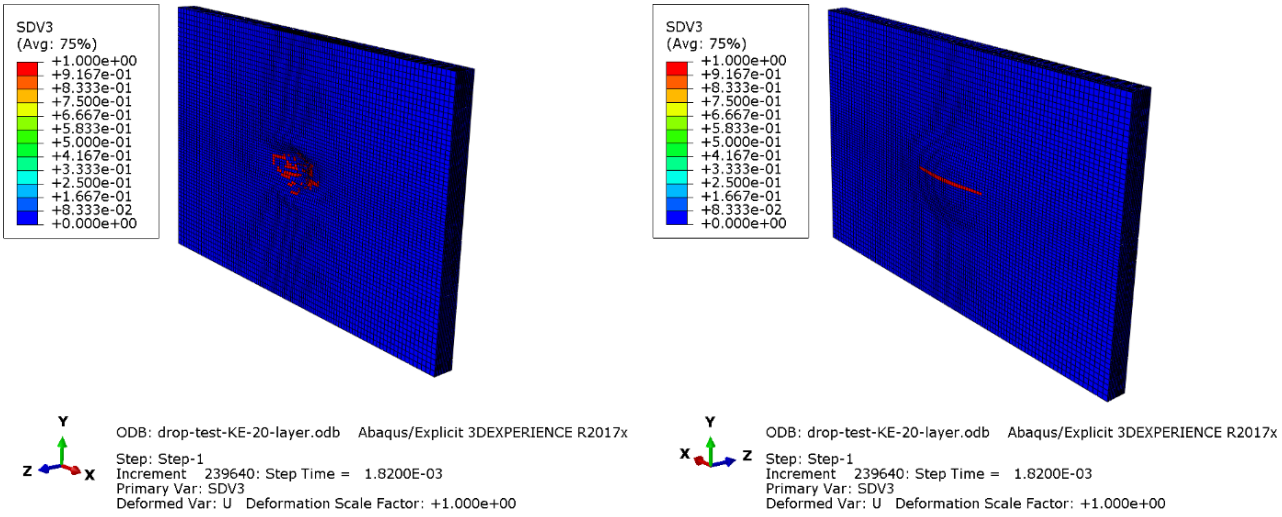


**(a)** front face **(b)** bottom face

**Figure 8:** Matrix tensile intralaminar damage of Kevlar

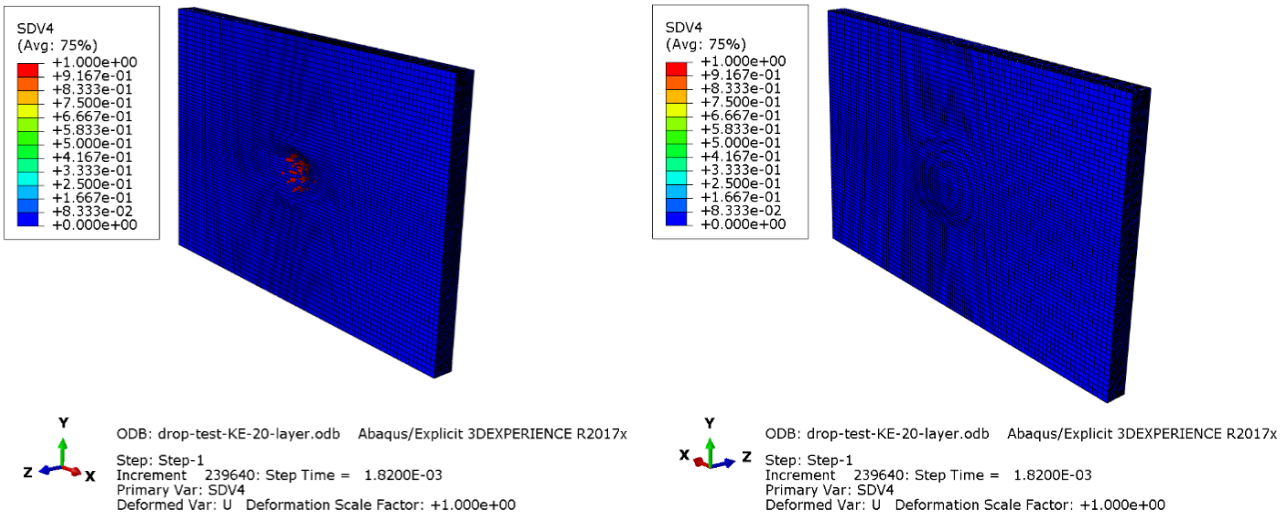


**(a)** front face **(b)** bottom face

**Figure 9:** Matrix compression intralaminar damage of Kevlar

tension and compression stresses, the matrix damage happens in the front and the backplate faces close to impact the region. The numerical model predicted failure modes as illustrated in Figures 8 and 9, where the SDV3 and SDV4 are matrix damage tension and matrix damage compression respectively. It can be seen that the numerical results have a good prediction of failure behavior compared with the experimental study.

## 5.3 Energy absorption

The energy absorption is considered a critical characteristic to estimate the structure's capability in many applications. This property is used to improve composite structure against the impact load and estimate their reliability in service. In low-velocity impact, the energy absorption dominates by both interlaminar and intralaminar fracture toughness. In this research, the same thermosetting polymer matrix is used as epoxy resin; on the other hand, two different types of fibers (Kevlar and Ultra High Molecular Weight Poly Ethylene) have different interlaminar fracture

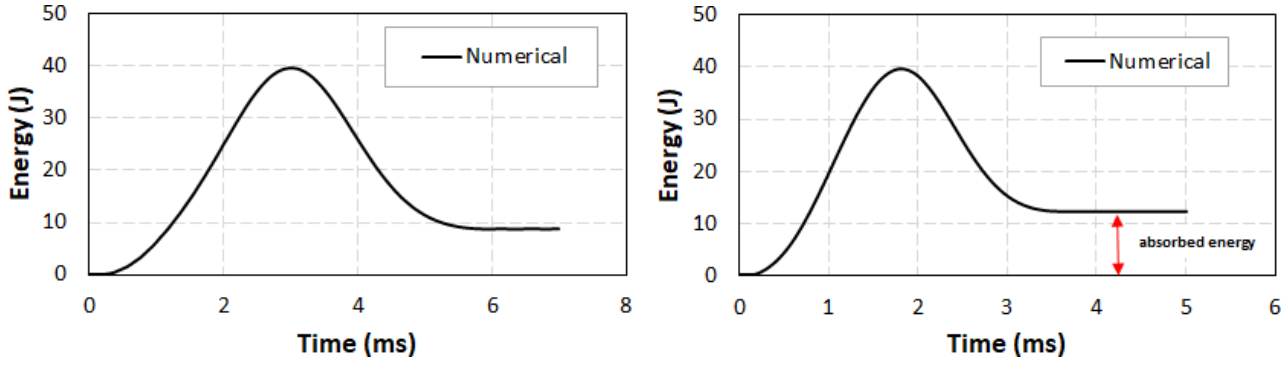


**(a)** 12-layers **(b)** 20-layers

**Figure 10:** Numerical energy absorption of Kevlar reinforced epoxy

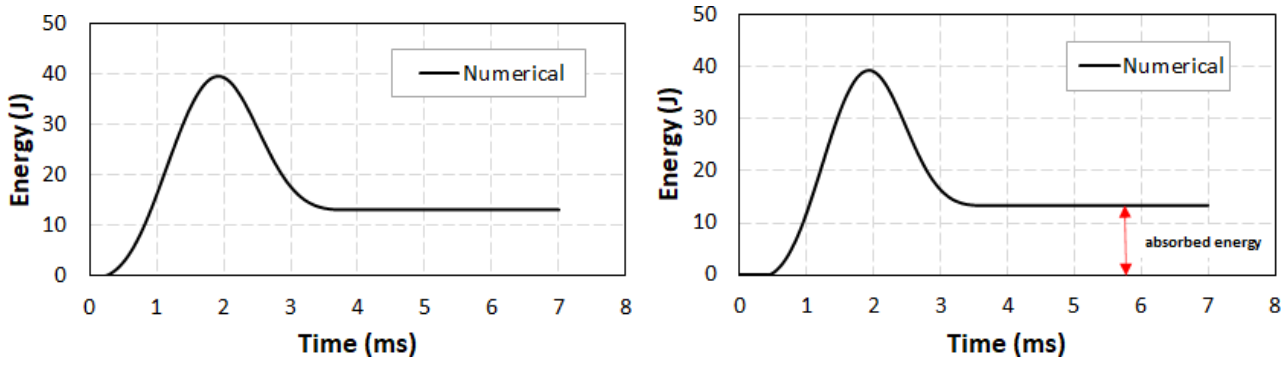


**(a)** 12-layers **(b)** 20-layers

**Figure 11:** Numerical energy absorption of UHMWPE reinforced epoxy

toughness with different interlaminar fracture toughness epoxy resin and have different density. The UHMWPE has a lower strain to failure and lower density than Kevlar, which indicates that it observed more energy absorption than Kevlar. Interlaminar and intralaminar have a significant effect on energy absorption. Numerically, the energy absorption was illustrated more clearly for both Kevlar and UHMWPE reinforced Epoxy in Figures 10 and 11.

## 6 Conclusions

This study implemented a low-velocity impact experimentally of two types of composite laminate with different thicknesses, Kevlar and UHMWPE reinforced epoxy, tested using a drop test machine. Also, a numerical model was modeled using the explicit finite element method/Abaqus software. The failure mechanism of the composite laminate was implemented based on interlaminar and intralaminar damage modes. The CZM was used to represent the interlaminar damage mode (delamination). Conversely, the intralaminar damage mode was modeled based on continuum damage mechanics. A user-defined subroutine (VUMAT) was adopted and integrated with Abaqus software to model the progressive degradation of the fiber and matrix of a composite laminate. The numerical results were compared with the experimental low-velocity impact test according to force time history and damage modes. A good agreement between the numerical and experimental results was noted. Finally, energy absorptions of the composite laminate have been examined to characteristic their capability to resist the impact loads.

**Funding information:** The authors state no funding involved.

**Author contributions:** All authors have accepted responsibility for the entire content of this manuscript and approved its submission.

**Conflict of interest:** The authors state no conflict of interest.

## References


[1] Randjbaran E, Zahari R, Jalil NA, Majid DL. Hybrid composite laminates reinforced with Kevlar/carbon/glass woven fabrics for ballistic impact testing. Sci World J. 2014;2014:413753.

[2] Gning PB, Tarfaoui M, Collombet F, Riou L, Davies P. Damage development in thick composite tubes under impact loading and influence on implosion pressure: experimental observations. Compos, Part B Eng. 2005;36(4):306–18.

[3] Tarfaoui M, Gning PB, Collombet F. Gning Papa Birame, Collombet F. Residual strength of damaged glass/epoxy tubular structures. J Compos Mater. 2007;41(18):2165–82.

[4] El Moumen A, Tarfaoui M, Lafdi K, Benyahia H; EL Moumen A. Tarfaoui M, Lafdi K, Benyahia H. Dynamic properties of carbon nanotubes reinforced carbon fibers/epoxy textile composites under low velocity impact. Compos, Part B Eng. 2017;125:1–8.

[5] Hassoon OH, Tarfaoui M, Alaoui A, El Malki EL, Moumen A. Experimental and numerical investigation on the dynamic response of sandwich composite panels under hydrodynamic slamming loads. Compos Struct. 2017;178:297–307.

[6] Richardson MO, Wisheart MJ. Review of low-velocity impact properties of composite materials. Compos, Part A Appl Sci Manuf. 1996;27(12):1123–31.

[7] Rodríguez Millán M, Moreno CE, Marco M, Santiuste C, Miguélez H. Numerical analysis of the ballistic behaviour of Kevlar® composite under impact of double-nosed stepped cylindrical projectiles. J Reinf Plast Compos. 2016;35(2):124–37.

[8] Oleiwi JK, Hamza MS, Abed MS. Study the tensile characteristics of elastomer composites reinforced with alumina and precipitated silica particles. Eng Tech J. 2015;33:1079–94.

[9] Li C, Zhang R, Jia J, Wang G, Shi Y. The low-velocity impact and post-impact properties of ultra-high-molecular-weight polyethylene fiber weft plain knitted structural composites. J Eng Fibers Fabrics. 2019;14:1–10.

[10] Oleiwi JK, Hamza MS, Abed MS. Improving the properties of the tire tread by adding sio2 and al2o3 to sbr rubber. Int J Appl Eng Res. 2010;5(9):1637–52.

[11] Rawat P, Singh KK. Damage tolerance of carbon fiber woven composite doped with mwcnts under low-velocity impact. Procedia Eng. 2017;173:440–6.

[12] Nayak N, Banerjee A, Panda TR. Numerical study on the ballistic impact response of aramid fabric- epoxy laminated composites by armor piercing projectile. Procedia Eng. 2017;173:230–7.

[13] Stopforth R, Adali S. Experimental study of bullet-proofing capabilities of Kevlar, of different weights and number of layers, with 9mm projectiles. Def Technol. 2019;15(2):186–92.

[14] Reddy TS, Reddy PR, Madhu V. Response of E-glass/Epoxy and dyneema composite laminates subjected to low and high-velocity impact. Procedia Eng. 2017;173:278–85.

[15] Schoeppner GA, Abrate S. Delamination threshold loads for low velocity impact on composite laminates. Compos, Part A Appl Sci Manuf. 2000;31(9):903–15.

[16] Yang B, Wang Z, Zhou L, Zhang J, Liang W. Experimental and numerical investigation of interply hybrid composites based on woven fabrics and PCBT resin subjected to low-velocity impact. Compos Struct. 2015;132:464–76.

[17] Meshi I, Amarilio I, Benes D, Haj-Ali R. Delamination behavior of UHMWPE soft layered composites. Compos, Part B Eng. 2016;98:166–75.

[18] Fadhil BM, Ahmed PS, Kamal AA. Improving mechanical properties of epoxy by adding multi-wall carbon nanotube. J Theor Appl Mech. 2016;54:551–60.

[19] Ahmed PS. Effect of impactor design on unidirectional and woven fiber reinforced composites. Sulaimani J Eng Sci. 2016;3(3):21–9.

[20] Sy BL. Low velocity impact assessment of flax and kevlar-flax fibre reinforced polymer laminates using experimental and numerical methods [dissertation]. Toronto: Ryerson University; 2017.

[21] Nachtane M, Tarfaoui M, Saifaoui D, El Moumen A, Hassoon OH, Benyahia H. Evaluation of durability of composite materials applied to renewable marine energy: case of ducted tidal turbine. Energy Rep. 2018;4:31–40.

[22] Hu Y, Liu W, Shi Y. Low-velocity impact damage research on CFRPs with Kevlar-fiber toughening. Compos Struct. 2016;216:127–41.

[23] Nachtane M, Tarfaoui M, Ait Mohammed M, Saifaoui D, El Moumen A. Effects of environmental exposure on the mechanical properties of composite tidal current turbine. Renew Energy. 2020;156:1132–45.

[24] Gürgen S. Low-velocity impact performance of UHMWPE composites consolidated with carbide particles. Arch Civ Mech Eng. 2020;20(2):38.

[25] Abed MS, Ahmed PS, Oleiwi JK, Fadhil BM. Low velocity impact of Kevlar and ultra high molecular weight polyethylene (UHMWPE) reinforced epoxy composites. Multidiscip Model Mater Struct. 2020;16(6):1617–30.

[26] Maziz A, Rechak S, Tarfaoui M. Comparative study of tubular composite structure subjected to internal pressure loading: analytical and numerical investigation. J Compos Mater. 2021;55(11):1517–33.

[27] Liu H, Liu J, Ding Y, Zhou J, Kong X, Bamber RK. Blackman, Anthony J. Kinloch, Brian G. Falzon, John P. Dear. Effects of impactor geometry on the low-velocity impact behaviour of fibre-reinforced composites: an experimental and theoretical investigation. Appl Compos Mater. 2020;27(5):533–53.

[28] Guo W, Xue P, Yang J. Nonlinear progressive damage model for composite laminates used for low-velocity impact. Appl Math Mech. 2013;34(9):1145–54.

[29] Hassoon OH, Tarfaoui M, El Moumen A. Progressive damage modeling in laminate composites under slamming impact water for naval applications. Compos Struct. 2017;167:178–90.

[30] El Moumen A, Tarfaoui M, Hassoon OH, Lafdi K, Benyahia H, Nachtane M. Experimental study and numerical modelling of low velocity impact on laminated composite reinforced with thin film made of carbon nanotubes. Appl Compos Mater. 2018;25(2):309–20.

[31] Camanho PP, Davila CG. Mixed-Mode decohesion finite elements for the simulation of delamination in composite materials. NASA Tech; 2002.

[32] Xin SH, Wen HM. A progressive damage model for fiber reinforced plastic composites subjected to impact loading. Int J Impact Eng. 2015;75:40–52.

[33] Gong XJ, Benzeggah ML. Determination of the mixed mode delamination toughness using an imposed displacement cantilever beam test method. In Bunsell AR, Jamet JF, Massiah A, editors. Fifth European Conference on Composite Materials; 1992 Apr

7-10; Bordeaux, France. 1992. p. 773–786.
[34] Soroush M, Fard KM, Shahravi M. MalekzadehFard K, Shahravi M. Finite element simulation of interlaminar and intralaminar damage in laminated composite plates subjected to impact. Lat Am J Solids Struct. 2018;15(6):1–20.